International Journal of Pharmaceutics: X 5 (2023) 100151

Contents lists available at ScienceDirect

International Journal of Pharmaceutics: X

journal homepage: www.sciencedirect.com/journal/international-journal-of-pharmaceutics-x

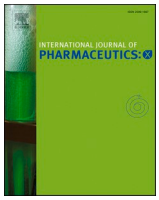

Drop-on-powder 3D printing of amorphous high dose oral dosage forms: Process development, opportunities and printing limitations

Nadine Gottschalk [a,b], Alicia Burkard [b], Julian Quodbach [a,c], Malte Bogdahn [b,*]

[a] Institute of Pharmaceutics and Biopharmaceutics, Heinrich Heine University, Düsseldorf, Germany
[b] Merck KGaA, Darmstadt, Germany
[c] Department of Pharmaceutics, Utrecht Institute for Pharmaceutical Sciences, Utrecht University, Netherlands

ARTICLE INFO

Keywords:
Drop-on-powder printing
Binder jetting
Amorphous solid dispersion
Solubility enhancement
3D Printing
Process development
Additive manufacturing

ABSTRACT

Drop-on-powder 3D printing is able to produce highly drug loaded solid oral dosage forms. However, this technique is mainly limited to well soluble drugs. The majority of pipeline compounds is poorly soluble, though, and requires solubility enhancement, e.g., via formation of amorphous solid dispersions. This study presents a detailed and systematic development approach for the production of tablets containing high amounts of a poorly soluble, amorphized drug via drop-on-powder 3D printing (also known as binder jetting). Amorphization of the compound was achieved via hot-melt extrusion using the exemplary system of the model compound ketoconazole and copovidone as matrix polymer at drug loadings of 20% and 40%. The milled extrudate was used as powder for printing and the influence of inks and different ink-to-powder ratios on recrystallization of ketoconazole was investigated in a material-saving small-scale screening. Crystallinity assessment was performed using differential scanning calorimetry and polarized light microscopy to identify even small traces of crystallinity. Printing of tablets showed that the performed small-scale screening was capable to identify printing parameters for the development of amorphous and mechanically stable tablets via drop-on-powder printing. A stability study demonstrated physically stable tablets over twelve weeks at accelerated storage conditions.

1. Introduction

Three-dimensional printing (3DP) demonstrated to be a capable set of techniques for the production of individualized solid oral dosage forms (SODFs) in the last years. 3DP or additive manufacturing (AM) is a generic term for the layer-by-layer production of three-dimensional (3D) objects from computer-based design. The creation of pharmaceutical SODFs in a layer-by-layer fashion can be done in several ways. There are techniques based on powder and liquid solidification as well as extrusion-based methods (Seoane-Viaño et al., 2021). What they have in common is fast adjustability of the 3D tablet design and by that adapting the dose and release properties (Goyanes et al., 2015; Windolf et al., 2021). Although, 3DP techniques have gained great popularity in the pharmaceutical research sector, for a long time Spritam® by Aprecia Pharmaceuticals was the only approved drug product by the U.S. Food and Drug Administration (FDA), which is produced using the technique drop-on-powder (DoP). Recently, Triastek received IND clearance for clinical studies by the FDA for their product T19, produced by Melt Extrusion Deposition (MED™) (Sen et al., 2021a). 3D printed products can be beneficial in clinical studies due to flexible dose adjustment and easy scalability (Sen et al., 2021a; Seoane-Viaño et al., 2021).

Besides the benefits for the manufacturing of clinical trial supply, 3DP techniques can also help solving the challenges of poor drug solubility. The majority of newly discovered compounds are poorly soluble and belong to the Biopharmaceutics Classification System (BCS) class II (Gala et al., 2020; Ting et al., 2018). A common strategy to enhance solubility and bioavailability of these compounds is the formulation of amorphous solid dispersions (ASD), where the amorphous active pharmaceutical ingredient (API) is kinetically stabilized in a polymer matrix. A kinetically stabilized system will eventually transform into a thermodynamically stable system, which means in case of an ASD that the amorphous API will recrystallize over time. Several factors such as the

Abbreviations: 3D, three-dimensional; 3DP, three-dimensional printing; AM, additive manufacturing; API, active pharmaceutical ingredient; ASD, amorphous solid dispersion; BCS, Biopharmaceutics Classification System; DoP, drop-on-powder; dpmm, dots per millimeter; DSC, differential scanning calorimetry; FDA, U.S. Food and Drug Administration; FDM, fused deposition modeling; HME, hot-melt extrusion; KTZ, ketoconazole; SODF, solid oral dosage form.

* Corresponding author.
E-mail address: malte.bogdahn@merckgroup.com (M. Bogdahn).

https://doi.org/10.1016/j.ijpx.2022.100151
Received 27 September 2022; Received in revised form 21 December 2022; Accepted 22 December 2022
Available online 23 December 2022

storage temperature, moisture content and remaining traces of crystallinity affect the physical stability (Shah et al., 2014). An ASD can be obtained by a variety of techniques among which hot melt extrusion (HME) is widely used. By the means of HME an API-polymer mixture is blended in a heated barrel and the API can become amorphous by either heating above the melting temperature or/and dissolving in the polymer matrix (Shah et al., 2014).

HME has been coupled frequently with the 3DP technique Fused Deposition Modeling (FDM), also a melt-extrusion based process, to achieve amorphous drug products. However, the mechanical properties of the filaments are a great issue (Fuenmayor et al., 2018; Ilyés et al., 2019; Nasereddin et al., 2018) and especially high drug loads may result in very brittle filaments, which are not printable using commercially available printers (Gottschalk et al., 2021). Therefore, the addition of plasticizers in the formulation is necessary in many cases, which can impair the physical stability of the ASD (Wei et al., 2020). Another promising 3DP technique is DoP. The DoP process can be described as an in-situ wet granulation, where small ink or binder droplets are jetted on thin powder layers resulting in fusion of the powder particles. The iterative process of powder spreading and ink application proceeds until the 3D objects is printed. Since the single powder particles are applied loosely onto each other, drug release from DoP printed SODFs benefits from the porous structure (Jennotte et al., 2020). In addition to that, high drug loads up to 70% are feasible, which is usually not the case for classical manufacturing techniques such as tableting due to poor compressibility of most APIs. However, in DoP printing tablet hardness and tablet friability can be impaired (Infanger et al., 2019; Wang et al., 2022a), which requires the usage of polymeric binders. The binder can be included in the ink (Chang et al., 2021; Goole and Amighi, 2016; Kozakiewicz-Latała et al., 2022; Sen et al., 2021b; Wang et al., 2021; Wilts et al., 2019) as well as in the powder bed (Wang et al., 2022b; Antic et al., 2021; Infanger et al., 2019; Tian et al., 2019; Wang et al., 2006; Zhang et al., 2021). The production of ASDs is possible by the means of DoP printing, if the API is included in the ink in combination with a volatile solvent due to fast evaporation from small droplets similar to spray-drying (Scoutaris et al., 2011; Wickström et al., 2015). The proportion of API in the ink depends on its solubility in the solvent and high API concentrations increase the likelihood of recrystallization of the API at the nozzle leading to nozzle clogging (Parhi, 2021). Furthermore, the achieved drug loads and dosages are low, being in the lower microgram-range up to a maximum of 5 mg (Clark et al., 2020; Raijada et al., 2013; Sharma et al., 2013). High drug loads, though, may be necessary to achieve high drug dosages by maintaining an adequate tablet size.

In the current literature, the use of DoP printing for high dose formulations is mainly described for highly soluble compounds. This study investigates the possibility of coupling HME with DoP printing by using hot-melt extruded ASDs as powder bed material. We present a systematic development approach for SODFs via DoP printing with the aim to produce fully amorphous dosage forms. Ketoconazole (KTZ), an antifungal agent with a poor solubility (22.2 µg/mL in Fasted State Simulated Intestinal Fluid (Auch et al., 2018) was used as model compound. As matrix polymer copovidone (Kollidon® VA64) was selected because of its suitability to produce ASDs with ketoconazole, especially in a melt-based approach (Auch et al., 2018), and because it has been reported to have strong binding properties when used as a solid binder in DoP printing (Antic et al., 2021; Chang et al., 2020). Water-based and water-free inks as well as various ink-to-powder ratios were assessed regarding their suitability to print high dose amorphous dosage forms. The selected key quality attributes for development were degree of recrystallization, physical stability and mechanical properties of the printed tablets.

2. Material and methods

2.1. Materials

KTZ was purchased from LGM Pharma (Boca Raton, USA). Copovidone (Kollidon® VA64, Vinylpyrrolidone-vinyl acetate copolymer) was purchased from BASF (Ludwigshafen, Germany). Methylene blue and the solvents ethanol, methanol and isopropyl alcohol (purity ≥99.9%) were provided by Merck (Darmstadt, Germany). Colloidal silicon dioxide was purchased from Evonik Industries (Essen, Germany).

2.2. Methods

2.2.1. Blending and extrusion

Two blends were prepared by weighing polymer and API and blending them using a Turbular® mixer (T2C, Willy A. Bachofen AG, Muttenz, Switzerland) for 15 min. Colloidal silicon dioxide was manually added to the premix and the mixture was sieved (mesh size: 1 mm) and blended again for 15 min. This was necessary to enable a uniform powder feeding of the KTZ-containing blends during extrusion. The composition of the blends is displayed in Table 1.

Extrusion was performed on a Pharma 11 twin-screw extruder (Thermo Fisher Scientific, Waltham, USA) with a screw configuration consisting of three kneading zones to achieve good mixing of API and polymer. A gravimetric feeder (Congrav® OP1 T) and conveyor belt from Brabender GmbH & Co. KG (Duisburg, Germany) were used. The conveyor belt was used to pull the extrudate strand to facilitate cooling. Extrudate was further cut into smaller pieces using diagonal pliers. A slow feed rate of 0.2 kg/h was chosen to prolong the residence time of the melt in the barrel and a high screw speed of 300 rpm to create a high input of mechanical energy to produce fully amorphous extrudates with homogeneously distributed API. Extrusion was performed above the melting point of KTZ (151 °C) and below the degradation temperature of 221 °C (Kanaujia et al., 2011). Barrel temperatures had to be adapted for each formulation to produce a self-supporting extrudate strand and are displayed in Table 2.

2.2.2. Milling and particle size determination

A typical layer height in DoP printing to achieve good resolution of printed objects is 100 µm (Chang et al., 2021; Wang et al., 2022b), hence, particles should be smaller than the intended layer height. Therefore, the aim was to produce particles <100 µm. For initial printing tests a small batch of approximately 15 g of extrudate (VA64-K0 and VA64-K40) was milled using a Tube Mill control (IKA, Staufen, Germany). The milling chamber was filled with a maximum of 5 g and milling was performed in steps of 1 min at 25,000 rpm with cooling steps of approximately 1 min in between to reduce thermal impact on the powder and prevent aggregation of particles. Each formulation was milled for 5–8 min in total. Milled extrudate was sieved with a mesh size of 200 µm. Using the Tube Mill, it was not possible to produce an appropriate amount of powder with a particle size <100 µm. As the initial screening was performed on trays with cavities deeper than 100 µm the powder was suitable. To reach a smaller particle size for the printing of tablets, an ultra-centrifugal mill (ZM 200, Retsch, Haan, Germany) was used. Formulations VA64-K20 and VA64-K40 were milled using a twelve-teeth rotor and a sieve with a mesh size of 200 µm with a distance ring at 10,000 rpm. Particle size was determined via dynamic image analysis using a Camsizer X2 (Retsch, Haan, Germany).

Table 1
Blend composition in wt%.

	VA64-K0	VA64-K20	VA64-K40
KTZ (%)	0	20	40
Copovidone (%)	100	79	59
Silicon dioxide (%)	0	1	1

Table 2
Extrusion parameters.

Formula-tion	Feed rate (kg/h)	Screw speed (rpm)	Zone 1 (°C)	Zone 2 (°C)	Zone 3 (°C)	Zone 4 (°C)	Zone 5 (°C)	Zone 6 (°C)	Zone 7 (°C)	Die (°C)
VA64-K0	0.2	200	80	180	180	180	180	180	180	180
VA64-K20	0.2	300	60	120	180	180	180	180	180	175
VA64-K40	0.2	300	60	120	160	160	160	150	150	150

The X-jet module was used. Dispersing pressure was set to 50 kPa and gap width to 4 mm. As D90 values of the milled extrudates were below 100 µm (supplementary material, Table S1), the whole powder fraction was used as powder bed material for printing.

2.2.3. Preparation of inks

Ink composition is displayed in Table 3. Ink was prepared by mixing the corresponding volumes. For pretests, methylene blue was added to the inks in a concentration of 0.16 mg/mL. No further characterization of the inks was performed.

2.2.4. Printing

2.2.4.1. Printer setup. Commercial binder jetting printers for pharmaceutical use are not available, yet. Therefore, a custom-made powder bed printer comprising an active powder reservoir, a roller, a powder bed with building platform and a printing station had to be modified. A schematic drawing of the printing process is displayed in Fig. 1.

The mechanical setup is controlled by an off-the-shelf motion control system compatible to the G-code standard. The build platform can move in xyz-direction, whereas the printing station is fixed. To create a powder layer the build plate is lowered by the intended layer height. For each printed layer the build platform moves under the orifice of a powder reservoir. A screw inside the reservoir distributes a powder pile onto the platform. In the next step, the platform moves at constant speed under the counter-rotating roller to spread the powder pile into a single layer. Hereafter, ink is deposited on the smoothened powder bed. The printing station was specifically designed. While industrial piezo inkjet printheads are suitable for large production setups with high throughput, they require advanced parameter tuning. For this study, modified HP C6602 cartridges (thermal printhead) were chosen because of their robustness. The cartridge was controlled via an Arduino Mega 2560 microcontroller board with an open-source extension board (Inkshield) and in-house developed firmware. The twelve nozzles of the printhead are arranged in a line with a length of 3.175 mm. Each of the twelve nozzles could be controlled individually. The motion controller of the printer generated a pulse signal to sync the print head controller to the printing motion. The distance between the nozzles and the powder bed was approximately 5 mm. The functionality of the nozzles was tested by checking the electrical resistance of each nozzle using a multimeter after each print. Broken nozzles are indicated by a greatly increased nozzle resistance.

The HP cartridge C6602 is a commercially available, prefilled printhead for 2D inkjet printing and therefore, had to be opened and thoroughly cleaned to allow filling with the prepared inks. Customized lids were printed from polylactic acid on a Prusa i3 MK3S (Prusa Research s.r.o., Prague, Czech Republic) and glued on the cartridge. The lids had been modified with a male luer-lock adapter to enable the connection to a vacuum pump. A meniscus vacuum of −1.96 mbar (−20 mm H_2O) was applied to prevent the ink from oozing. Approximately 10 mL of ink were filled in the cartridge using a syringe to ensure a comparable filling level for all experiments.

2.2.4.2. Determination of droplet volume. The droplet volume of the inks containing methylene blue was determined by jetting 1800 droplets per nozzle into a UV transparent 96 well plate (Corning, New York, USA). Ink was diluted with 200 µL of demineralized water and absorption of methylene blue at 665 nm was measured using a microplate reader (Spark, Tecan, Männedorf, Switzerland). A calibration in the wells with 200 µL of five aqueous solutions of methylene blue in a range from 1.6 to 5.7 µg/mL was performed ($n = 3$). The droplet volume was calculated from the jetted amount of methylene blue and the total number of droplets. Five replicate tests were performed for each ink.

2.2.4.3. Parameter screening. For the initial print parameter screening only the print station and the build platform were used. Extrudate milled using the Tube Mill was spread manually using cardboard on small trays with cavities of 500 µm depth. Various ink-to-powder ratios were evaluated, by printing single layer objects with a fixed layer height. The ink-to-powder ratio is referred to as dots per mm in printing direction (dpmm). All twelve nozzles were used to print a band, wherefore the distance between the droplet orthogonal to the printing direction was fixed. Material and parameter combination are listed in Table 4. The build plate moved at constant speed in x-direction below the print head during droplet generation. Additional tests were performed to evaluate the influence of enhanced drying on printed layers using a 1 kW halogen lamp (Philips, Amsterdam, Netherlands) on samples printed with E70 at 50 dpmm at full and half intensity for 0.5, 5 and 10 min. The lamp was placed approximately 15 cm above the freshly printed samples.

2.2.4.4. Printing of tablets. For printing of multilayer objects, the combination of printing station, build platform, powder reservoirs and roller was used. Cylindrical tablets (height: 2.4 mm, diameter: 10 mm) were designed in Fusion 360 (Autodesk, Farnborough, United Kingdom) and

Table 3
Ink composition (*v*/v%) and ink properties from literature.

Ink	Composition (v/v%)				Ink properties at 20 °C[1]		
	Methanol	Ethanol	Isopropyl alcohol	Purified water	Vapor pressure (kPa)	Surface tension (mN/m)	Viscosity (mPa*s)
M100	100	–	–	–	13.0[a]	22.6[b]	0.6[b]
E70	–	70	–	30	5.9[c]	27.5[d]	1.2[c]
IPA90	–	–	90	10	–	22.2[e]	2.7[f]

[1]Literature data:
[a] (Gibbard and Creek, 1934).
[b] (Wanchoo and Narayan, 1992).
[c] Safety data sheet "Ethyl alcohol 70% v/v"
[d] (Khattab et al., 2012).
[e] (Vazquez et al., 1995).
[f] (Pang et al., 2007).

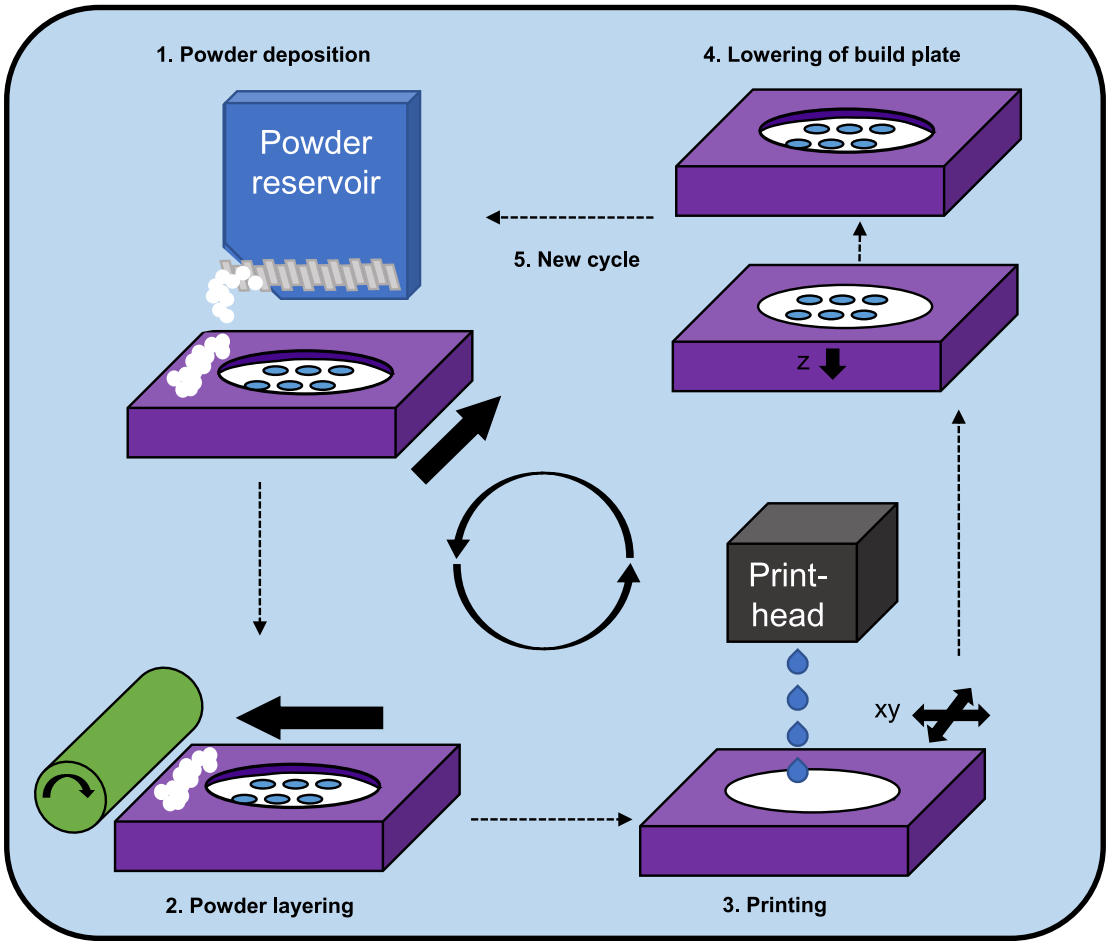

Fig. 1. Schematic drawing of printing process.

Table 4
Screening of printing parameters.

Screening experiment	Material	Ink-to-powder ratio (dpmm)	Printing length (mm)	Inks
… to estimate ink-to-powder ratio	VA64-K0	10, 50, 100, 150, 200, 250	5	E70
	VA64-K0	30, 40, 50, 60, 70, 80	5	E70
	VA64-K40	30, 40, 50, 60, 70, 80	5	E70
… to assess the influence of ink-to-powder ratio on recrystallization	VA64-K40	30, 40, 50, 60	60	M100
	VA64-K40	30, 40, 50, 60	60	E70
	VA64-K40	40, 50, 60	60	IPA90
… to assess the influence of drying with lamp on recrystallization	VA64-K40	50	60	E70

saved in a binary stereolithography file format (.stl) with high resolution. The file resembling the tablet geometry was converted into printing and motion data via a specifically developed script written in Python 3.7. The script accepted all print settings as input parameters. The motion commands were saved as G-code file and imported into the motion control software of the printer. The corresponding graphical information were sent to the print head controller via USB connection during the print job. The powder was automatically deposited from the powder reservoir and spread via the counter-rotating roller set to 350 rpm. The platform moved at a speed of 600 mm/min. Layer height was set to 0.1 mm. After ink jetting, the powder bed was left to rest for 15 s before the next powder layering step. Twelve tablets were printed at the same time. The powder bed was dried in a vacuum drier (VacuTherm VT6060MBL, Thermo Fisher Scientific, Waltham, USA) at <100 mbar at room temperature overnight.

2.2.5. Storage

To assess the physical stability, printed tablets were stored in open glass vessels in a desiccator with silica gel at 40 °C in a climate chamber for 2, 4 and 12 weeks (KBF 240, Binder, Tuttlingen, Germany).

2.2.6. Polarized light microscopy

Single layer objects and printed tablets were crushed using mortar and pestle prior to analysis. Furthermore, the top layer of tablets was cut off using a cutter knife, to allow a 2D view on the samples. Samples were qualitatively analyzed using polarized light microscopy (IX73P1F, Olympus, Tokyo, Japan) at 5× and 10× magnification with regards to traces of crystallinity and their location in the tablet. Images were recorded using Olympus cellSens standard software (version: 1.18).

2.2.7. Differential scanning calorimetry (DSC)

Crystallinity assessment of samples was performed using a DSC 1 (Mettler Toledo, Gießen, Germany). Neat substances, blends, milled extrudates and ground printed samples were analyzed. Approximately 7–9 mg were weighed into a 100 µL aluminum pan and hermetically sealed. The lid was pierced prior to analysis using the automatic piercing unit. Samples containing methylene blue were heated twice from 0 °C to

200 °C, samples without methylene blue were heated from 0 °C to 170 °C at heating and cooling rates of 10 K/min. Tests were performed in triplicate.

2.2.8. Tablet hardness

Printed tablets were analyzed using an Erweka tablet hardness tester (THB 125, Erweka, Langen, Germany). Tablets were placed in the hardness tester in such a way that the force acted in the direction of printing. Tests were performed in triplicate. In case of VA64-K20 tablets printed with E70, ten tablets were tested. Tensile strength was calculated according to Pitt and Heasley, 2013.

3. Results and discussion

The approach of using already amorphous API as powder bed material has not been described in the literature so far. The single steps from ink selection and parameter optimization to the printing process and characterization of printed tablets will be described in the following sections. A flowchart of the work performed in this study is displayed in Fig. 2.

3.1. Small-scale prescreening: identification of printing parameters

3.1.1. Ink and ink-to-powder ratio screening

Aim of initial printing pretests was to test whether the milled hot-melt extrudate from copovidone was suitable as solid binder and to which extend recrystallization of the amorphously embedded API in the polymer matrix would occur by varying ink-to-powder ratios. Tests were performed with highly drug loaded material (40% *w*/w). The high proportion of API molecules in the extrudate makes the formulation more susceptible to recrystallization. It was assumed that this would facilitate differentiation between the different settings and inks. Pretests were further designed to consume as little time and material as possible.

First, single layer objects were printed with ink E70 to estimate the approximate amount of ink necessary to fuse extrudate particles from VA64-K0 and VA64-K40 leading to mechanically stable flakes. It was assumed that parameters leading to stable flakes would lead to mechanically stable tablets or can be used as starting point for tablet optimization. The dye methylene blue was used to visualize ink distribution in the flakes. Initially, a broad range of ink-to-powder ratios was selected and used with VA64-K0. With regards to potential recrystallization of KTZ in the following experiments, ink-to-powder ratios where selected, which were as low as possible but still resulted in stable flakes. Visual assessment of the samples (Fig. 3) indicated excess amounts of ink at volumes >100 dpmm. Here, the amount of ink was too high to be absorbed by the powder material leading to fusion of ink droplets and the formation of an “ink pool”. In contrast, 10 dpmm did not lead to fusion of the powder particles and the printed sample was very fragile. Consequently, a range from 30 to 80 dpmm was selected. The samples were assessed on whether they could be picked up and removed from the

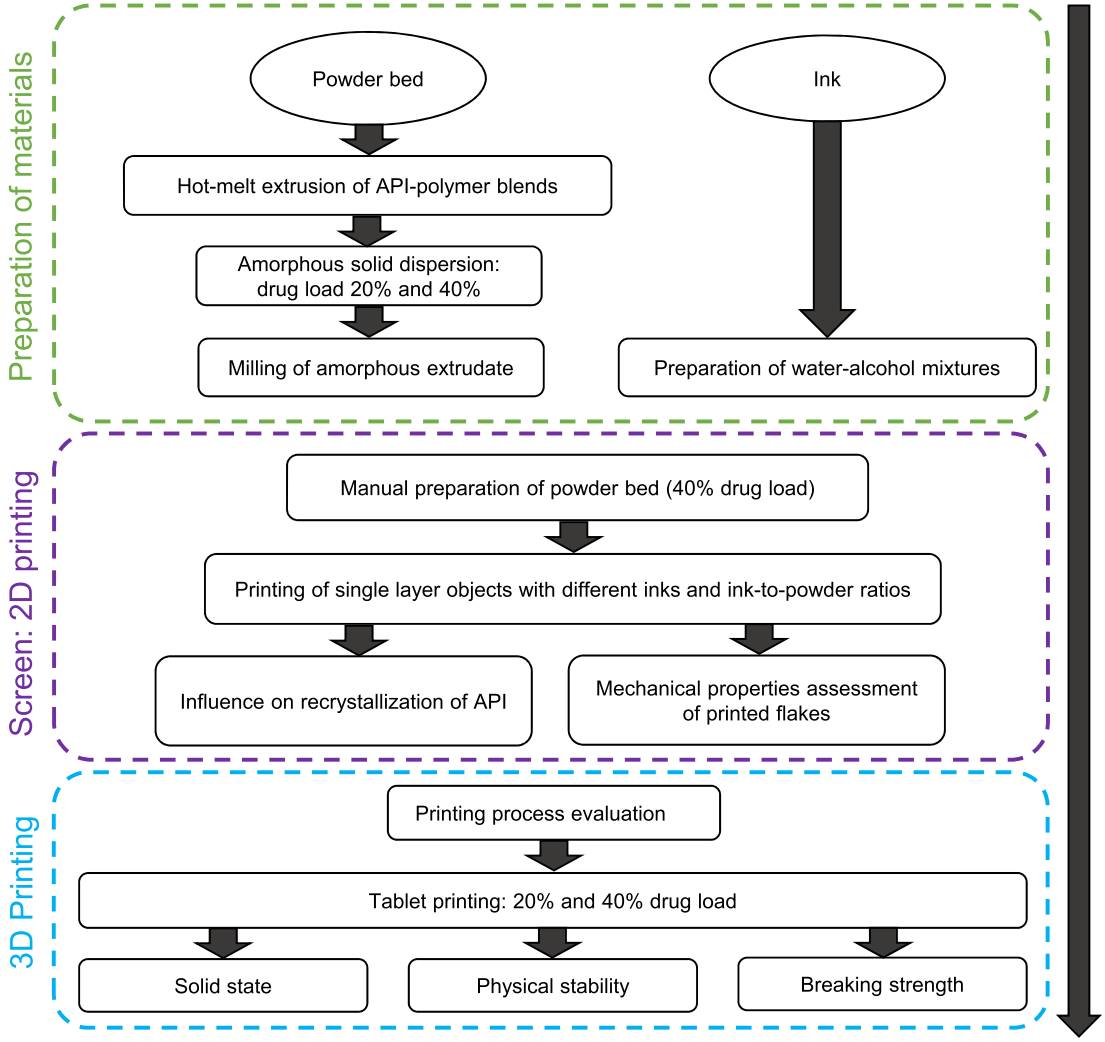

Fig. 2. Flowchart of the development approach in this study.

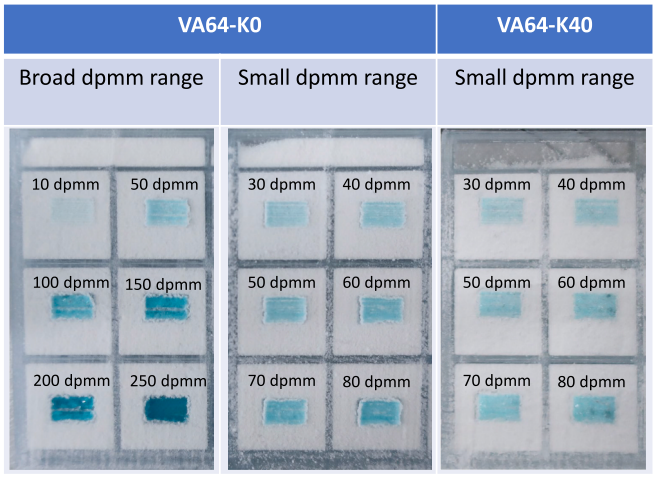

Fig. 3. Various ink-to-powder ratios in a range of 10–250 dpmm with E70 ink containing methylene blue on milled extrudate (VA64-K0 and VA64-K40). (For interpretation of the references to colour in this figure legend, the reader is referred to the web version of this article).

powder bed in one piece using tweezers. Tests were performed using VA64-K0 and VA64-K40, which resulted in stable flakes starting at 40 dpmm in case of VA64-K0 and 50 dpmm in case of VA64-K40, indicating that due to the reduction of the amount of solid binder, mechanical stability was impaired. In case of VA64-K0 the samples slightly bent upwards. The warping effect is not desired in powder bed printing since it may lead to removal of printed layers during recoating of a new powder layer, stopping the printing process (Tian et al., 2019). The reason for warping is that upon contact with water, polymers like copovidone undergo swelling due to sorption of water (Li et al., 2011). Hence, warping was stronger at higher ink-to-powder ratios. However, during swelling, inter-particular bonds are created, which contribute to the mechanical strength of the samples. Subsequent drying, which does not occur uniformly over the whole wetted area as the edges dry faster, results in contraction and warping. To ensure a continuous printing process and mechanically stable samples, a sweet spot regarding the ink-to-powder ratio has to be identified. In case of VA64-K40, strong warping was only present at high ink-to-powder ratios >70 dpmm, possibly due to a lower proportion of the binder copovidone.

Next to the E70 ink another water-based ink, IPA90, and a water-free ink, M100, were tested in a range of 40–60 dpmm. Visual assessment of the prints (supplementary material Fig. S1) with inks containing ethanol and methanol indicated good distribution of the ink on the powder surface, whereas the IPA90 ink led to neither a good distribution nor mechanically stable samples. The droplet volume of IPA90 was smaller (IPA90: 72 pL ± 2 pL, E70: 124 pL ± 3 pL, M100: 131 pL ± 4 pL) A likely reason is the more as twice as high viscosity of the IPA90 ink (Table 3). Due to the small droplet volume and high viscosity, it is unlikely that proper particle fusion and good mechanical strength of tablets will be achieved. Therefore, IPA90 was excluded from following experiments.

3.1.2. *Assessment of recrystallization behavior*

In the next step, the effects on recrystallization of the inks E70 and M100 in various ink-to-powder ratios were assessed. Extruded and milled powder was analyzed in advance and was fully amorphous prior to the screening (supplementary material Fig. S2). In addition, the miscibility of API and polymer was demonstrated using DSC. A single glass transition was observed, which indicates a miscible system (supplementary material, Fig. S3). Assessment of single layer objects via polarized light microscopy (Fig. 4) showed birefringence starting from 50 dpmm, indicating recrystallization. To rule out that birefringence was possibly a result of light refraction where particles had fused, samples were compared to printed single layers of VA64-K0 (supplementary material Fig. S4). Here, no such birefringence was observed indicating that the birefringence in VA64-K40 was due to recrystallization upon contact with the inks. The proportion of recrystallization appeared to be slightly higher for the water-containing ink E70, which is possibly a result of a lower vapor pressure and slower evaporation of the solvent (Table 3). The droplet volume of E70 and M100 was almost identical. The observed recrystallization was too low to be detected via DSC (data not shown). The limit of detection had been determined in prior experiments (Gottschalk et al., 2021) and was found to be 2.0% leading us to assume that the proportion of crystallinity is below this

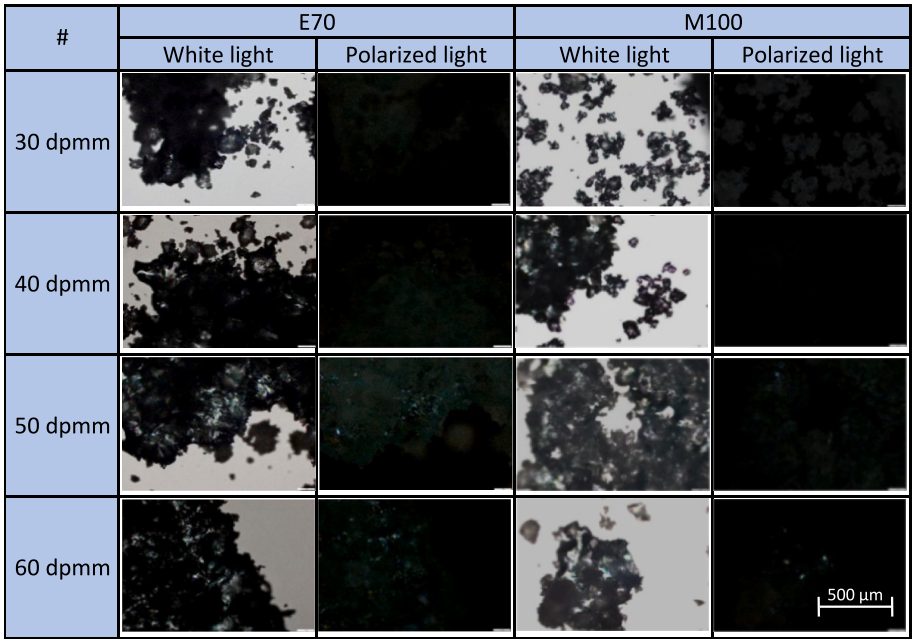

Fig. 4. Influence of ink-to-powder ratios on recrystallization of amorphous KTZ at 40% drug load comparing E70 and M100 containing methylene blue. Microscope images with white and polarized light at 10× magnification. (For interpretation of the references to colour in this figure legend, the reader is referred to the web version of this article).

limit. It has to be pointed out that variations between printheads may lead to variations of the droplet volume. Several printheads were used in this study since single nozzles stopped working occasionally, indicated by an increased electrical nozzle resistance.

Additional drying with a halogen lamp directly after printing was performed to evaluate whether this would reduce recrystallization due to faster evaporation. To our surprise, the opposite was observed and drying induced recrystallization (Fig. 5). After using the lamp for 30 s at maximum intensity, samples were not dry and it appeared that the energy input provided the activation energy for recrystallization. All samples demonstrated recrystallization to a greater extend compared to samples, which had not been dried. The intensity was reduced to prevent initial recrystallization but even though samples were dry after 5 and 10 min of drying, recrystallization could not be prevented and an additional drying step was considered not suitable regarding this process.

Pretests already indicated that the amorphous extrudate was susceptible to recrystallization upon wetting with the inks, possibly due to higher molecular mobility in the wetted areas. It became also apparent that mechanical strength decreased with decreasing ink-to-powder ratios, which requires the definition of optimal conditions. It has to be mentioned that only a single layer was printed and the drying rate will be impaired when printing a multilayer object. In contrast, samples will probably be mechanically more stable since fusion of the particles will not only occur in xy-direction but also in z-direction. In the pretests, milled extrudate with a particle size range of 100–200 µm was used. Particle sizes <100 µm were used for printing of multilayer objects. This should further lead to an enhanced mechanical stability of the printed samples because of additional binding locations. Considering all these aspects, an ink-to-powder ratio of 30 dpmm was selected for printing of multilayer objects. Methylene blue was not used in follow-up experiments. Comparative experiments were performed with a E70 ink without methylene blue leading to comparable results regarding recrystallization and mechanical properties of printed layers (supplementary material, Fig. S5).

3.2. Transfer of identified printing parameters to multilayer objects

3.2.1. Printing process

The results from the pre-screening in 3.1 were transferred to the actual printing process of multilayer dosage forms. Observations in the following section are described for the formulation VA64-K20. Conclusions from these initial printing experiments were transferred to formulation VA64-K40. No differences in powder behavior between VA64-K20 and VA64-K40 were observed.

First, powder layer spreadability was assessed using the roller. Milled extrudate showed good powder-layering properties: the powder layers were smooth and homogenous in a broad range of roller speed settings (50–400 rpm) without throwing the powder over the roll during powder distribution or shearing powder against each other. A uniform powder bed is important to ensure quality of tablets. Powder bed defects may impair the mechanical strength of the printed tablets and, when the API is included in the powder bed, will probably lead to poor mass and dosing conformity of the tablets. Occasionally, extrudate particles attached to the roll (Fig. 6), resulting in furrows on the powder surface. This phenomenon was observed more frequently when the milled extrudate was exposed to air humidity for longer periods of time. Drying of the powder could reduce this effect but since the polymer copovidone is highly hygroscopic (Liu et al., 2013) and due to the great surface area of the fine powder, absorption can occur fast. To prevent this effect, working in an environment with controlled air humidity would have been necessary. Since this was not possible, particles that had adhered to the roll had to be removed manually using a wiper to ensure a smooth powder bed.

Differences in terms of processability were observed during testing of the inks E70 and M100. M100 printed at 30 dpmm resulted in a smooth first layer, whereas in case of E70 the first layer showed warping at the edges of the printed area as already observed during the prescreening. Due to warping, the printed layers were removed by the roller in the next powder layering step and the print job had to be aborted. To overcome this phenomenon, the ink-to-powder ratio was decreased to 10 dpmm and the roller speed was varied. These attempts were not successful, indicating that barely visible warping effects can interrupt the printing process. In addition to that, the initial build plate layer height was adapted stepwise to create a very thin first powder layer (0.2 mm) so the first printed layer would be in contact to the build plate (Fig. 7). Adhesion of the first printed layer prevented warping and printing was feasible. However, printing was only feasible in a narrow first layer height range: first layer heights ≥0.3 mm resulted in removal of the first printed layer whereas first layer height ≤ 0.1 mm led to a strong adhesion to the build plate, making removal of printed tablet without breaking them impossible.

3.2.2. Tablet properties

Tablets were printed from formulations VA64-K20 and VA64-K40 with the inks E70 and M100 and a representative tablet is displayed in Fig. 8a. Tablets were white and slightly yellowish where the ink wetted the powder bed. Three darker stripes were visible on the tablet surface, which is a result of the printhead moving four times over the powder bed to cover the whole area. The twelve nozzles of the printhead are arranged in a line with a length of 3.175 mm and the tablet diameter was 10 mm. It was observed that if only a single nozzle would break during printing, the tablets would fall apart at this location (supplementary

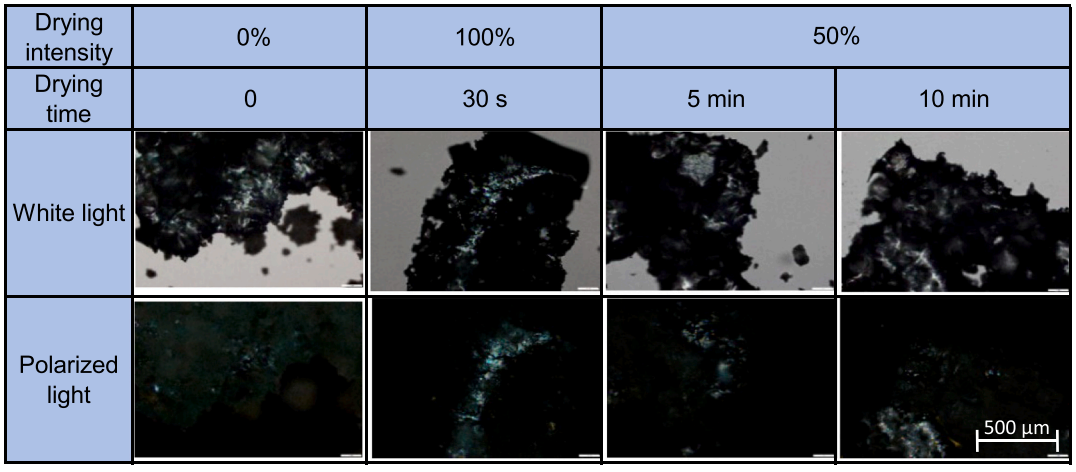

Fig. 5. Influence of drying intensity and time on recrystallization of KTZ at 40% drug load at 50 dpmm printed with E70.

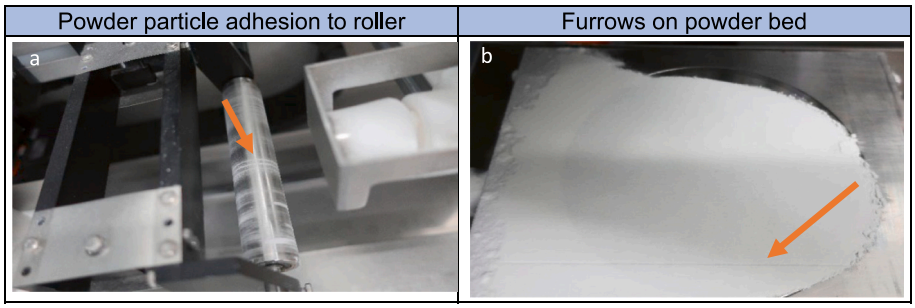

Fig. 6. Adhesion of powder particles on distributing roller (a) and the resulting furrows in the powder bed (b).

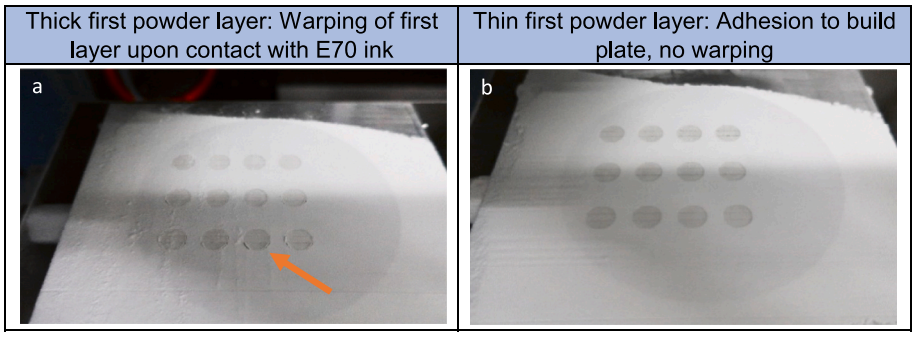

Fig. 7. Warping of first layer (orange arrow) when printing on a thick first powder layer (a) and a thin first powder layer (b).

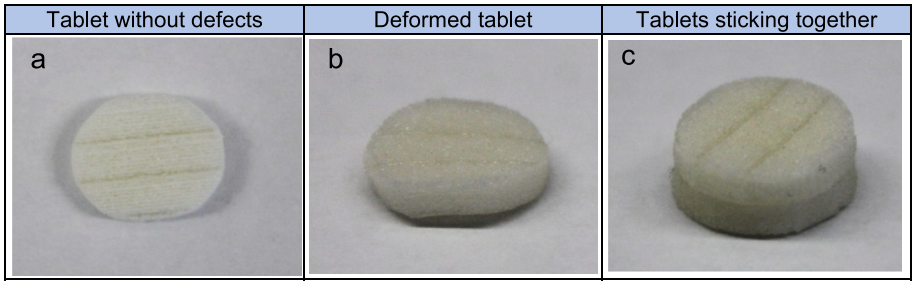

Fig. 8. Table without defects (VA64-K20 printed with E70) after printing and drying (a), deformed tablet (b) and tablets sticking together after 2 weeks of storage (c).

material, Fig. S6). Therefore, the slicer had been programmed to produce a slight overlap on print passes to prevent tablets falling apart. This resulted in areas with higher ink-to-powder ratio visible as stripes on the tablets.

Tablets printed with E70 had nearly twice the tensile strength of tablets printed with M100 (Table 5) and are close to 1 MPa, which is a reported target value in the literature (Leane et al., 2015). As already described in Section 3.2.1., strong warping, which had been observed with E70, probably correlates with strong particle fusion. The tensile strength was independent from the proportion of solid binder in the formulation highlighting the importance of ink selection for the mechanical properties of printed tablets.

The tensile strength of tablets printed with E70 increased during storage. It was also observed that printed tablets before storage showed a strong decrease in glass transition temperature compared to the neat milled extrudate (54.2 °C ± 0.9 °C vs. 34.0 °C ± 12.1 °C for VA64-K20). A pronounced endothermic event was observed at 90–100 °C in DSC data indicating the evaporation of water. Water acts as powerful plasticizer and reduces the glass transition temperature (Pereira et al., 2019). Samples were kept at 40 °C during storage, which was above the glass transition temperature of the printed tablets, and it is likely that higher molecular mobility of the polymer resulted in an enhanced fusion of particles increasing the tablet strength. Contributing to that, some of the tablets were slightly deformed and occasionally sticked together (Fig. 8b and c). The glass transition temperature increased during storage to 69.4 °C ± 0.6 °C indicating a loss of water.

Regarding the recrystallization in dependence of the ink, printing of VA64-K40 with E70 resulted in enhanced recrystallization of KTZ compared to M100 as already indicated in the pre-screening. The effect

Table 5
Tensile strength of tablet with 20% and 40% drug load printed with E70 and M100 ($n = 3$).

Formulation	Ink	Tablet tensile strength at stability time point (MPa) ± SD			
		T0	2 weeks	4 weeks	12 weeks
VA64-K20	E70	0.93 ± 0.30*	1.76 ± 0.31*	2.33 ± 0.28*	1.83 ± 0.47*
	M100	0.64 ± 0.19	0.76 ± 0.12	0.70 ± 0.41	0.79 ± 0.13
VA64-K40	E70	1.05 ± 0.21	N/A	N/A	N/A
	M100	0.51 ± 0.14	0.56 ± 0.15	0.64 ± 0.13	0.59 ± 0.13

* $n = 10$.

on recrystallization was more pronounced than in the pre-screening (Fig. 9) and 2.8% crystalline KTZ was detected via DSC. The reason for this is most likely the lower surface area-to-volume ratio of stacked wet powder layers resulting in a slower drying process compared to single layer objects.

By means of the fast-evaporating solvent methanol the degree of recrystallization was minimized but could not be completely eliminated. Even small traces of solvent can impair the physical stability of a formulation, which was the case of VA64-K40 tablets printed with M100. Additional recrystallization occurred after 12 weeks of storage at accelerated conditions. Analysis of single tablet layers indicated that recrystallization was localized to where material had been directly wetted by the ink (Fig. 10). Areas in between showed no recrystallization. As a result of the fixed nozzle spacing, areas in between are wetted only indirectly by ink diffusion leading to a lower moisture content.

In a supersaturated formulation with a drug load of 40%, the distance between API molecules is small. The addition of liquid even at small amounts increases the mobility of the molecules in the wetted areas, facilitating recrystallization. Therefore, DoP printing is considered unsuitable for the production of physically stable tablets at such high drug loads. Here, an approach where the tablet contains loose powder and only the shell and top and bottom layers are printed as described by Yu et al. (2009) would be conceivable. Mechanical strength and physical stability of the inner phase would have to be assessed separately in this case.

At a lower drug load of 20%, the difference between the two inks was less pronounced. Tablets printed with M100 were fully amorphous and remained amorphous during storage. Regarding tablets printed with E70, in the ground samples a few particles >100 µm were detected that contained a high number of crystalline spots (Fig. 9). These large particles were a result of the printing process and fusion of particles, where, due to the slicer settings, overlapping of printed lines occurred. After storage for twelve weeks at accelerated conditions crystals were still only localized there (Fig. 10) and samples were fully amorphous in areas where no overlapping occurred. The crystalline amount was too low to be detected via DSC.

The low drug load as well as the high porosity of the tablets contribute to the enhanced physical stability. This example shows that even small amounts of excess ink and recrystallization can be compensated when using lower drug loads. An overview on all formulations and their results can be found in the supplementary material (Table S2).

4. Conclusion

In this study, we demonstrated that DoP printing of hot-melt extruded ASD powder containing KTZ was successful. The screening method developed for this purpose has proven to be capable of identifying suitable printing parameters. Printing of single layer objects was time-efficient and material-saving and close observations of the material behavior were a good indicator of a successful printing process and quality of the printed tablets. Tablets printed in this study showed satisfactory results in terms of mechanical strength and solid-state properties. Even though only small amounts of ink were used, tablets exhibited high tensile strengths up to 2.33 MPa when printed with a water-based ink. Fully amorphous and physically stable tablets were produced with 20% drug load printed with a water-free ink. A higher drug load of 40% KTZ was also feasible, but the presence of small crystalline traces induced recrystallization after twelve weeks of storage at accelerated conditions, demonstrating the limits of this approach. However, at drug loads of 20% small crystalline traces did not induce recrystallization during storage as they remained localized, which was attributed to the porous structure of the tablets. Further evaluations on additional APIs and polymers need to be performed.

DoP printing has so far been rarely used for the formulation of ASDs. Our approach shows that DoP printing coupled with HME has the potential to produce amorphous high dose tablets. This technique represents an alternative to other 3DP techniques such as FDM, which is often limited by the mechanical properties of the feedstock materials. Furthermore, the combination of an amorphous and highly porous formulation is advantageous for the formulation of poorly soluble drugs as it will increase solubility and dissolution and thereby likely enhance oral bioavailability. In a follow-up study, we will compare this technique to the FDM process in terms of processability and dosage form performance.

Funding

Parts of this work were supported by the German Federal Ministry of Education and Research [grant number 13XP5064].

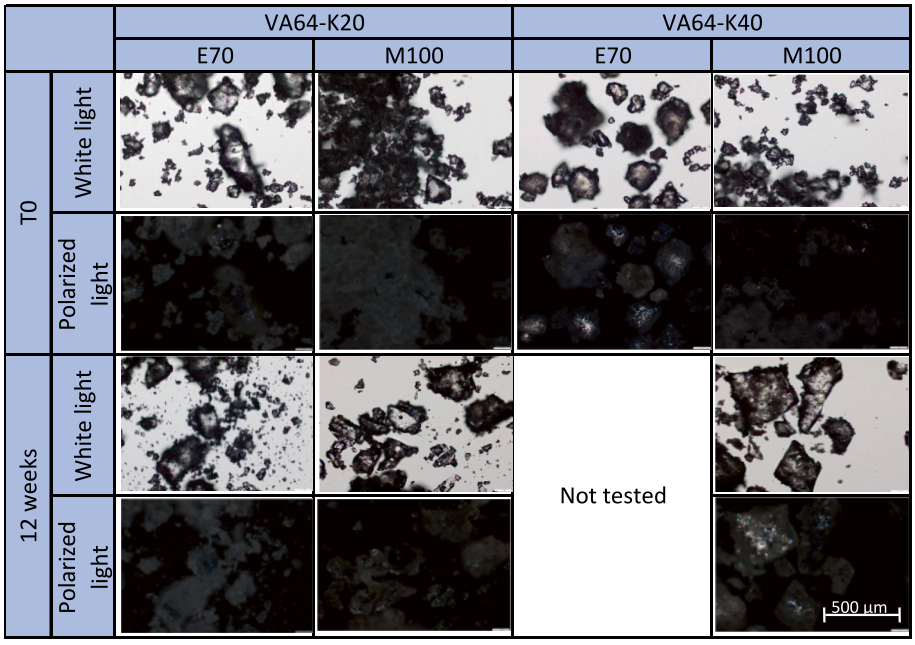

Fig. 9. Ground tablets with 20% and 40% drug load printed with E70 and M100. Images using white and polarized light at 10× magnification.

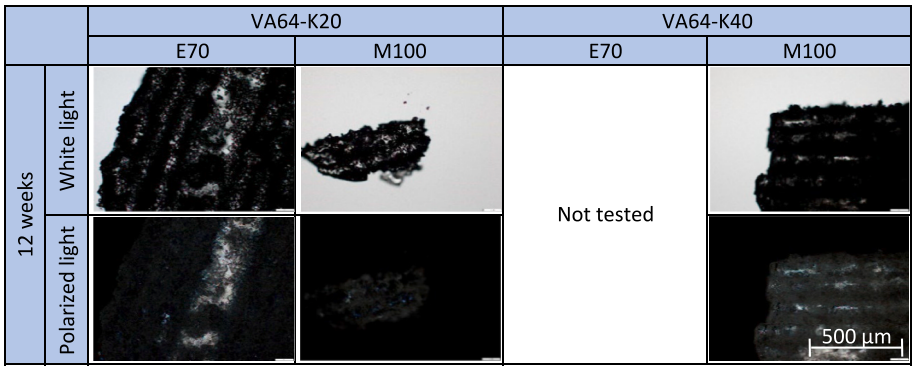

Fig. 10. Microscope images of tablet fragments at 5× magnification using white and polarized light.

CRediT authorship contribution statement

Nadine Gottschalk: Conceptualization, Investigation, Methodology, Formal analysis, Writing – original draft, Visualization. **Alicia Burkard:** Investigation, Formal analysis. **Julian Quodbach:** Conceptualization, Supervision, Writing – review & editing. **Malte Bogdahn:** Conceptualization, Supervision, Writing – review & editing.

Declaration of Competing Interest

The authors declare the following financial interests/personal relationships which may be considered as potential competing interests:

Malte Bogdahn has patent Process for the manufacture of a solid pharmaceutical administration form pending to Merck Patent GmbH. Nadine Gottschalk has patent Process for the manufacture of a solid pharmaceutical administration form pending to Merck Patent GmbH. Julian Quodbach has patent Process for the manufacture of a solid pharmaceutical administration form pending to Merck Patent GmbH.

Data availability

No data was used for the research described in the article.

Acknowledgements

The authors would like to thank Marcel Wedel for his technical support during the experiments. The authors would also like to thank the German Federal Ministry of Education and Research, as parts of this work were funded through the initiative ProMatLeben (grant number 13XP5064).

Appendix A. Supplementary data

Supplementary data to this article can be found online at https://doi.org/10.1016/j.ijpx.2022.100151.

References

Antic, A., Zhang, J., Amini, N., Morton, D.A.V., Hapgood, K.P., Ft, F., 2021. Screening pharmaceutical excipient powders for use in commercial 3D binder jetting printers. Adv. Powder Technol. 32, 2469–2483. https://doi.org/10.1016/j.apt.2021.05.014.

Auch, C., Harms, M., Mäder, K., 2018. Melt-based screening method with improved predictability regarding polymer selection for amorphous solid dispersions. Eur. J. Pharm. Sci. 124, 339–348. https://doi.org/10.1016/j.ejps.2018.08.035.

Chang, S., Wan, S., Kowsari, K., Shetty, A., Sorrells, L., Sen, K., Nagapudi, K., Chaudhuri, B., Ma, A.W.K., 2020. Binder-Jet 3D printing of indomethacin-laden pharmaceutical dosage forms. J. Pharm. Sci. 109, 3054–3063. https://doi.org/10.1016/j.xphs.2020.06.027.

Chang, S., Jin, J., Yan, J., Dong, X., Chaudhuri, B., 2021. Development of a pilot-scale HuskyJet binder jet 3D printer for additive manufacturing of pharmaceutical tablets. Int. J. Pharm. 605, 120791 https://doi.org/10.1016/j.ijpharm.2021.120791.

Clark, E.A., Alexander, M.R., Irvine, D.J., Roberts, C.J., Wallace, M.J., Yoo, J., Wildman, R.D., 2020. Making tablets for delivery of poorly soluble drugs using photoinitiated 3D inkjet printing. Int. J. Pharm. 578, 118805 https://doi.org/10.1016/j.ijpharm.2019.118805.

Ethyl Alcohol, 70% v/v; MSDS No. VT270 [Online]; Val Tech Diagnostics: Zelienople, PA, USA, August 13, 2013; http://www.labchem.com/tools/msds/msds/VT270.pdf. (accessed January 4, 2023).

Fuenmayor, E., Forde, M., Healy, A., Devine, D., Lyons, J., McConville, C., Major, I., 2018. Material considerations for fused-filament fabrication of solid dosage forms. Pharmaceutics 10, 44. https://doi.org/10.3390/pharmaceutics10020044.

Gala, U.H., Miller, D.A., Williams, R.O., 2020. Harnessing the therapeutic potential of anticancer drugs through amorphous solid dispersions. Biochim. Biophys. Acta - Rev. Cancer 1873, 188319. https://doi.org/10.1016/j.bbcan.2019.188319.

Gibbard, H.F., Creek, J.L., 1934. Vapor pressure of Methanol from 288.15 to 337.65 K. J. Chem. Eng. Data 19, 308–310. https://doi.org/10.1021/je60063a013.

Goole, J., Amighi, K., 2016. 3D printing in pharmaceutics: a new tool for designing customized drug delivery systems. Int. J. Pharm. 499, 376–394. https://doi.org/10.1016/j.ijpharm.2015.12.071.

Gottschalk, N., Bogdahn, M., Harms, M., Quodbach, J., 2021. Brittle polymers in Fused Deposition Modeling: an improved feeding approach to enable the printing of highly drug loaded filament. Int. J. Pharm. 597, 120216 https://doi.org/10.1016/j.ijpharm.2021.120216.

Goyanes, A., Robles Martinez, P., Buanz, A., Basit, A.W., Gaisford, S., 2015. Effect of geometry on drug release from 3D printed tablets. Int. J. Pharm. 494, 657–663. https://doi.org/10.1016/j.ijpharm.2015.04.069.

Ilyés, K., Kovács, N.K., Balogh, A., Borbás, E., Farkas, B., Casian, T., Marosi, G., Tomuță, I., Nagy, Z.K., 2019. The applicability of pharmaceutical polymeric blends for the fused deposition modelling (FDM) 3D technique: Material considerations–printability–process modulation, with consecutive effects on in vitro release, stability and degradation. Eur. J. Pharm. Sci. 129, 110–123. https://doi.org/10.1016/j.ejps.2018.12.019.

Infanger, S., Haemmerli, A., Iliev, S., Baier, A., Stoyanov, E., Quodbach, J., 2019. Powder bed 3D-printing of highly loaded drug delivery devices with hydroxypropyl cellulose as solid binder. Int. J. Pharm. 555, 198–206. https://doi.org/10.1016/j.ijpharm.2018.11.048.

Jennotte, O., Koch, N., Lechanteur, A., Evrard, B., 2020. Three-dimensional printing technology as a promising tool in bioavailability enhancement of poorly water-soluble molecules: a review. Int. J. Pharm. 580, 119200 https://doi.org/10.1016/j.ijpharm.2020.119200.

Kanaujia, P., Lau, G., Ng, W.K., Widjaja, E., Hanefeld, A., Fischbach, M., Maio, M., Tan, R.B.H., 2011. Nanoparticle Formation and growth during in Vitro Dissolution of Ketoconazole Solid Dispersion. J. Pharm. Sci. 100, 2876–2885. https://doi.org/10.1002/jps.22491.

Khattab, I.S., Bandarkar, F., Fakhree, M.A.A., Jouyban, A., 2012. Density, viscosity and surface tension of water+ethanol mixtures from 293 to 323 K. Korean J. Chem. Eng. 29, 812–817. https://doi.org/10.1007/11814-011-0239-6.

Kozakiewicz-Latała, M., Nartowski, K.P., Dominik, A., Malec, K., Gołkowska, A.M., Złocińska, A., Rusińska, M., Szymczyk-Ziółkowska, P., Ziółkowski, G., Górniak, A., Karolewicz, B., 2022. Binder jetting 3D printing of challenging medicines: from low dose tablets to hydrophobic molecules. Eur. J. Pharm. Biopharm. 170, 144–159. https://doi.org/10.1016/j.ejpb.2021.11.001.

Leane, M., Pitt, K., Reynolds, G., 2015. A proposal for a drug product Manufacturing Classification System (MCS) for oral solid dosage forms. Pharm. Dev. Technol. 20, 12–21. https://doi.org/10.3109/10837450.2014.954728.

Li, J., Tao, L., Dali, M., Buckley, D., Gao, J., Hubert, M., 2011. The effect of the physical states of binders on high-shear wet granulation and granule properties: a mechanistic approach toward understanding high-shear wet granulation process. Part II. Granulation and granule properties. J. Pharm. Sci. 100, 294–310. https://doi.org/10.1002/jps.22261.

Liu, J., Cao, F., Zhang, C., Ping, Q., 2013. Use of polymer combinations in the preparation of solid dispersions of a thermally unstable drug by hot-melt extrusion. Acta Pharm. Sin. B 3, 263–272. https://doi.org/10.1016/j.apsb.2013.06.007.

Nasereddin, J.M., Wellner, N., Alhijjaj, M., Belton, P., Qi, S., 2018. Development of a simple mechanical screening method for predicting the feedability of a pharmaceutical FDM 3D printing filament. Pharm. Res. 35, 151. https://doi.org/10.1007/s11095-018-2432-3.

Pang, F.-M., Seng, C.-E., Teng, T.-T., Ibrahim, M.H., 2007. Densities and viscosities of aqueous solutions of 1-propanol and 2-propanol at temperatures from 293.15 K to 333.15 K. J. Mol. Liq. 136, 71–78. https://doi.org/10.1016/j.molliq.2007.01.003.

Parhi, R., 2021. A review of three-dimensional printing for pharmaceutical applications: Quality control, risk assessment and future perspectives. J. Drug Deliv. Sci. Technol. 64, 102571 https://doi.org/10.1016/j.jddst.2021.102571.

Pereira, B.C., Isreb, A., Forbes, R.T., Dores, F., Habashy, R., Petit, J.-B., Alhnan, M.A., Oga, E.F., 2019. "Temporary Plasticiser": a novel solution to fabricate 3D printed patient-centred cardiovascular "Polypill" architectures. Eur. J. Pharm. Biopharm. 135, 94–103. https://doi.org/10.1016/j.ejpb.2018.12.009.

Pitt, K.G., Heasley, M.G., 2013. Determination of the tensile strength of elongated tablets. Powder Technol. 238, 169–175. https://doi.org/10.1016/j.powtec.2011.12.060.

Raijada, D., Genina, N., Fors, D., Wisaeus, E., Peltonen, J., Rantanen, J., Sandler, N., 2013. A step toward development of printable dosage forms for poorly soluble drugs. J. Pharm. Sci. 102, 3694–3704. https://doi.org/10.1002/jps.23678.

Scoutaris, N., Alexander, M.R., Gellert, P.R., Roberts, C.J., 2011. Inkjet printing as a novel medicine formulation technique. J. Control. Release 156, 179–185. https://doi.org/10.1016/j.jconrel.2011.07.033.

Sen, K., Mehta, T., Sansare, S., Sharifi, L., Ma, A.W.K., Chaudhuri, B., 2021a. Pharmaceutical applications of powder-based binder jet 3D printing process – a review. Adv. Drug Deliv. Rev. 177, 113943 https://doi.org/10.1016/j.addr.2021.113943.

Sen, K., Mukherjee, R., Sansare, S., Halder, A., Kashi, H., Ma, A.W.K., Chaudhuri, B., 2021b. Impact of powder-binder interactions on 3D printability of pharmaceutical tablets using drop test methodology. Eur. J. Pharm. Sci. 160, 105755 https://doi.org/10.1016/j.ejps.2021.105755.

Seoane-Viaño, I., Trenfield, S.J., Basit, A.W., Goyanes, A., 2021. Translating 3D printed pharmaceuticals: from hype to real-world clinical applications. Adv. Drug Deliv. Rev. 174, 553–575. https://doi.org/10.1016/j.addr.2021.05.003.

Shah, N., Sandhu, Ha, Choi, D.S., Chokshi, H., Malick, A.W. (Eds.), 2014. Dissolution of Amorphous Solid Dispersions: Theory and Practice. Springer. https://doi.org/10.1007/978-1-4939-1598-9_15.

Sharma, G., Mueannoom, W., Buanz, A.B.M., Taylor, K.M.G., Gaisford, S., 2013. In vitro characterisation of terbutaline sulphate particles prepared by thermal ink-jet spray freeze drying. Int. J. Pharm. 447, 165–170. https://doi.org/10.1016/j.ijpharm.2013.02.045.

Tian, P., Yang, F., Yu, L., Lin, M.-M., Lin, W., Lin, Q., Lv, Z., Huang, S., Chen, Y., 2019. Applications of excipients in the field of 3D printed pharmaceuticals. Drug Dev. Ind. Pharm. 45, 905–913. https://doi.org/10.1080/03639045.2019.1576723.

Ting, J.M., Porter, W.W., Mecca, J.M., Bates, F.S., Reineke, T.M., 2018. Advances in polymer design for enhancing oral drug solubility and delivery. Bioconjug. Chem. 29, 939–952. https://doi.org/10.1021/acs.bioconjchem.7b00646.

Vazquez, G., Alvarez, E., Navaza, J.M., 1995. Surface tension of alcohol water + water from 20 to 50 °C. J. Chem. Eng. Data 40, 611–614. https://doi.org/10.1021/je00019a016.

Wanchoo, R.K., Narayan, J., 1992. Excess properties of (Methanol + Toluene or p -xylene) binary liquid mixture. Phys. Chem. Liq. 25, 15–26. https://doi.org/10.1080/00319109208027283.

Wang, C.-C., Tejwani, M.R., Roach, W.J., Kay, J.L., Yoo, J., Surprenant, H.L., Monkhouse, D.C., Pryor, T.J., 2006. Development of near zero-order release dosage forms using three-dimensional printing (3-DPTM) technology. Drug Dev. Ind. Pharm. 32, 367–376. https://doi.org/10.1080/03639040500519300.

Wang, Z., Han, X., Chen, R., Li, J., Gao, J., Zhang, H., Liu, N., Gao, X., Zheng, A., 2021. Innovative color jet 3D printing of levetiracetam personalized paediatric preparations. Asian J. Pharm. Sci. 16, 374–386. https://doi.org/10.1016/j.ajps.2021.02.003.

Wang, Y., Müllertz, A., Rantanen, J., 2022a. Additive manufacturing of solid products for oral drug delivery using binder jetting three-dimensional printing. AAPS PharmSciTech 23, 196. https://doi.org/10.1208/s12249-022-02321-w.

Wang, Y., Müllertz, A., Rantanen, J., 2022b. Structured approach for designing drug-loaded solid products by binder jetting 3D printing. Eur. J. Pharm. Sci. 178, 106280 https://doi.org/10.1016/j.ejps.2022.106280.

Wei, C., Solanki, N.G., Vasoya, J.M., Shah, A.V., Serajuddin, A.T.M., 2020. Development of 3D Printed Tablets by Fused Deposition Modeling using polyvinyl Alcohol as Polymeric Matrix for Rapid Drug Release. J. Pharm. Sci. 109, 1558–1572. https://doi.org/10.1016/j.xphs.2020.01.015.

Wickström, H., Palo, M., Rijckaert, K., Kolakovic, R., Nyman, J.O., Määttänen, A., Ihalainen, P., Peltonen, J., Genina, N., de Beer, T., Löbmann, K., Rades, T., Sandler, N., 2015. Improvement of dissolution rate of indomethacin by inkjet printing. Eur. J. Pharm. Sci. 75, 91–100. https://doi.org/10.1016/j.ejps.2015.03.009.

Wilts, E.M., Ma, D., Bai, Y., Williams, C.B., Long, T.E., 2019. Comparison of linear and 4-arm star poly(vinyl pyrrolidone) for aqueous binder jetting additive manufacturing of personalized dosage tablets. ACS Appl. Mater. Interfaces 11, 23938–23947. https://doi.org/10.1021/acsami.9b08116.

Windolf, H., Chamberlain, R., Quodbach, J., 2021. Predicting drug release from 3D printed oral medicines based on the surface area to volume ratio of tablet geometry. Pharmaceutics 13, 1453. https://doi.org/10.3390/pharmaceutics13091453.

Yu, D., Branford-White, C., Yang, Y.-C., Zhu, L., Welbeck, E.W., Yang, X., 2009. A novel fast disintegrating tablet fabricated by three-dimensional printing. Drug Dev. Ind. Pharm. 35, 1530–1536. https://doi.org/10.3109/03639040903059359.

Zhang, J., Allardyce, B.J., Rajkhowa, R., Wang, X., Liu, X., 2021. 3D printing of silk powder by Binder Jetting technique. Addit. Manuf. 38, 101820 https://doi.org/10.1016/j.addma.2020.101820.